NASA Technical Memorandum 85960

Studies of Low-Mass Star Formation with the Large Deployable Reflector

A.G.G.M. Tielens and D.J. Hollenbach

July 1984

National Aeronautics and
Space Administration

NASA Technical Memorandum 85960

Studies of Low-Mass Star Formation with the Large Deployable Reflector

A. G. G. M. Tielens,
D. J. Hollenbach, Ames Research Center, Moffett Field, California

National Aeronautics and
Space Administration

Ames Research Center
Moffett Field, California 94035

This Page Intentionally Left Blank

SYMBOLS

a_T	isothermal sound speed in collapsing cloud
A_v	visual extinction
c	speed of light
D	distance of observer from accretion disk
G	gravitational constant
h	Planck constant
I_ν	blackbody specific intensity
k	Boltzmann's constant
L_s	shock luminosity
$\dot{M}$	mass accretion rate of protostar
M_c	mass of protostellar core
n	hydrogen nucleus number density
n_s	hydrogen nucleus number density at the shock front
n_w	hydrogen nucleus number density of protostellar wind
N_H	column density of hydrogen nuclei
Q	extinction efficiency of dust
r	distance from protostar
R_{ev}	distance to which grains evaporate
R_{max}	distance from protostar to outer radius of accretion disk
R_{out}	distance from protostar to surface of cloud
R_s	distance from protostar to accretion shock
S_ν	integrated emission observed from disk
T_{ev}	evaporation temperature of dust
T_o	cloud temperature at collapse
v_s	speed of accretion shock
v_w	speed of the wind from a protostellar source

λ wavelength of radiation

σ surface mass density of accretion disk

τ optical depth of dust

Ω solid angle of accretion disk as seen by observer

SUMMARY

In this report we estimate the far-infrared and submillimeter continuum and line emissions from regions of low-mass star formation and evaluate the capabilities of the proposed Large Deployable Reflector (LDR) for studying this problem. The LDR is a large space telescope designed for this wavelength range; construction is planned for the 1990s. It is concluded that the LDR will be able to probe the temperature, density, and chemical structure, and the velocity field in the collapsing envelopes of these protostars. In addition, the LDR will be useful in studying the accretion shocks on the cores and circumstellar disks of low-mass protostars, and will be able to detect shocks driven by protostellar winds.

1. INTRODUCTION

Stars form through the gravitational collapse of interstellar molecular clouds. Although we now possess a wealth of information on the properties of molecular clouds, on the circumstances under which stars form, and on the newly formed stars once they become visible, little is known about the actual process of star formation. This is mainly a result of the lack of an adequate observational tool. As discussed in this report, the Large Deployable Reflector (LDR), an orbiting, far-infrared, 20-m-diam telescope, will be extremely useful in studies of collapsing molecular clouds.

In this report we concentrate on application of the LDR to studies of the formation of low-mass stars and the possibility of the formation of planets around them. First, we review our theoretical knowledge of the star-formation process, emphasizing those areas in which the LDR may serve to fill in the large gaps in our understanding (sec. 2). Then we describe two types of observational programs possible with the LDR: studies of the continuum emission (sec. 3), and studies of the line emission (sec. 4) of collapsing molecular clouds.

The authors wish to acknowledge the support of the Advanced Program Office, NASA Headquarters, under RTOP 159-41-01.

2. THEORY OF STAR FORMATION

The star-formation process starts with the fragmentation of a parent molecular cloud into a number of clumps. The physics of this fragmentation process is poorly understood. It is currently believed that turbulence, as well as magnetic fields, plays an important role (Myers, 1983; Mestel, 1977). Table 1 lists the average properties observed in different types of molecular clouds and clumps in molecular clouds. Definite signs of star formation (e.g., infrared emission from protostars, T Tauri stars, maser emission, and compact H II regions) have been detected in all of these types of clouds (except for diffuse H I clouds). It should be noted, however, that in molecular clouds, the star-formation activity might be confined to the cores.

TABLE 1.- PROPERTIES OF MOLECULAR CLOUDS

Type	L, $L_\odot$	n, cm^{-3}	T, K	M, $M_\odot$
Diffuse H I cloud[a]	5	20	80	2.5×10^2
Bok globule[b]	.9	7×10^3	10	5.0×10^2
Small molecular cloud[c]	5	8×10^3	10	9.8×10^4
Dense core[d]	.1	$>3\times10^4$	10	>3
Giant molecular cloud[e]	25	7×10^2	10	1.0×10^6
Warm cores[f]	.3	$>1\times10^5$	30	2.6×10^2

References: [a]Spitzer (1978); [b]Martin and Barrett (1978); [c]Snell (1981); [d]Myers and Benson (1983); [e]Solomon (1978); [f]Evans (1978).

Collapse of a Spherically Symmetric Cloud

The one-dimensional collapse of a spherically symmetric cloud is relatively simple to calculate. As a consequence, much theoretical work has been done on this simplified problem, and its characteristics are relatively well understood (see the review by Larson, 1978).

The collapse of a cloud starts isothermically. When the cloud becomes optically thick to visible radiation, it heats up. The collapse of a cloud is nonhomologous, that is, the center collapses faster than the outside (Larson, 1972). This results in a core-envelope structure in which the envelope falls freely in on a core, which is already in hydrostatic equilibrium. At the interface, these two zones are separated by an accretion shock. In this shock front, nearly all of the kinetic energy of the in-falling material is transformed into internal energy of the gas and is then almost completely radiated away. An important difference between the formation of low-mass and high-mass stars is that in the formation of high-mass stars nuclear reactions commence in the core (e.g., the core reaches the main sequence), while the envelope is still accreting. This is not so in the formation of low-mass stars. In low-mass stars, most of the generated luminosity is gravitational energy released in the accretion shock. It should also be noted that radiation pressure is unimportant for the structure of the collapsing envelope around low-mass protostars.

The velocity of the flow into the accretion shock, v_s, is given by

$$v_s = \left(\frac{2GM_c}{R_s}\right)^{1/2} = 300\left(\frac{M_c}{1M_\odot}\right)^{1/2}\left(\frac{3\times10^{11}\ cm}{R_s}\right)^{1/2} \text{ km/sec} \qquad (1)$$

The shock luminosity L_s is equal to

$$L_s = \frac{GM_c\dot{M}}{R_s} \qquad (2)$$

where M_c is the mass in the core, R_s is the radius of the shock, G is the gravitational constant, and $\dot{M}$ is the mass accretion rate. For the isothermal collapse of a gaseous sphere whose initial state is not far removed from the critical state for gravitational stability, the mass accretion rate is approximately given by

$$\dot{M} = \frac{a_T^3}{G} = 5.7\times10^{-6}\left(\frac{T_o}{10\ K}\right)^{3/2}\ M_\odot\ yr^{-1} \tag{3}$$

where a_T is the isothermal sound speed (Shu, 1977; Stahler et al., 1980). This approximation for the mass accretion rate is reasonably accurate until the later phases of the collapse when the boundary condition becomes dominant. The shock luminosity can now be written as

$$L_s = 44\left(\frac{M_c}{1M_\odot}\right)\left(\frac{T_o}{10\ K}\right)^{3/2}\left(\frac{3\times10^{11}\ cm}{R_s}\right)L_\odot \tag{4}$$

where $R_s = 3\times10^{11}$ cm is a typical value for the radius of the accretion shock in the collapse of a 1-$M_\odot$ cloud (Stahler et al., 1980), except for the very first phase after the formation of the hydrostatic core. A good approximation of the number density n(r) of the freely falling gas is given by

$$n(r) = n_s\left(\frac{R_s}{r}\right)^{3/2} \tag{5}$$

where n_s is the density at the shock front. This can also be written as

$$n(r) = \frac{\dot{M}}{[4\pi(2GM_c)^{1/2}m_H r^{3/2}]} = 7\times10^{12}\left(\frac{T_o}{10\ K}\right)^{3/2}\left(\frac{M_c}{1M_\odot}\right)^{-1/2}\left(\frac{r}{3\times10^{11}\ cm}\right)^{-3/2}\ cm^{-3} \tag{6}$$

Generally, the collapsing envelope will consist of two zones. In the outer zone, the opacity is dominated by dust. In the inner zone, the dust has evaporated. The opacity in this zone, caused solely by gas, is four orders of magnitude less than in the outer zone. The two zones are separated by a sharp transition region where the dust is destroyed. The evaporation temperature of the most-refractory grain present in the interstellar medium, graphite, is about 2000 K (Salpeter, 1977). Typically this yields for the radius of the transition zone, R_{ev}, about 10^{13} cm. Figure 1 shows a sketch of these different zones in a collapsing cloud, and table 2 lists their approximate sizes.

The spectral appearance of a collapsing cloud is critically dependent on the optical depth, $\tau(\lambda)$, of the envelope. The principal contribution to the opacity comes from the dust:

$$\tau(\lambda) = \int_{R_{ev}}^{R_{out}} n_d(r)\langle\pi a^2\rangle Q(\lambda)dr \tag{7}$$

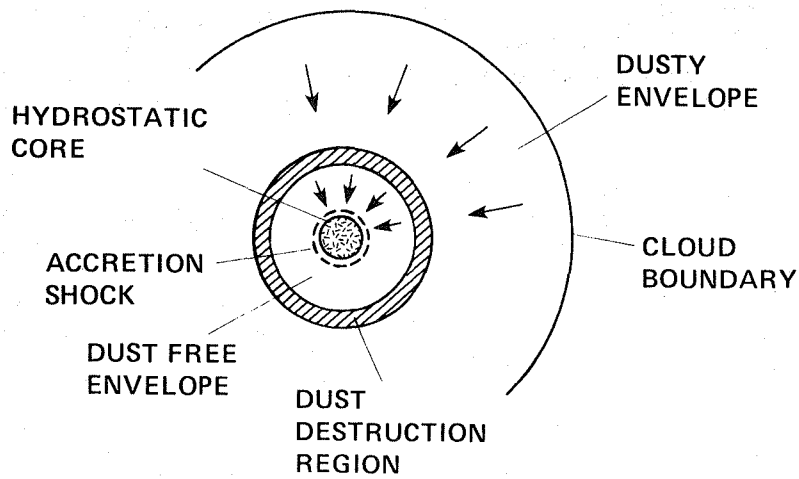

Figure 1.- A schematic of the structure of a spherically symmetric collapsing cloud.

TABLE 2.- SIZES OF THE DIFFERENT ZONES IN A COLLAPSING SPHERICALLY SYMMETRIC CLOUD

Zone	r, cm
Central core	3×10^{10}
Accretion shock	3×10^{11}
Dust-free envelope	10^{13}
Dusty envelope	10^{17}

where n_d, πa^2, and $Q(\lambda)$ are the number density, mean surface area, and extinction efficiency of the dust, respectively. Using equation (6) and

$$\frac{A_V}{N_H} = \frac{1}{2}\, n_d(r) \langle \pi a^2 \rangle \frac{Q(V)}{n(r)} \tag{8}$$

we find

$$\tau(\lambda) = 7.6\times10^{2}\left(\frac{T_o}{10\ K}\right)^{3/2}\left(\frac{M_c}{1M_\odot}\right)^{-1/2}\left(\frac{R_{ev}}{10^{13}\ cm}\right)^{-1/2}\frac{Q(\lambda)}{Q(V)} \tag{9}$$

Obviously, a collapsing cloud will be very thick, optically, in the visible region of the spectrum during most of the collapse phase. When most of the envelope has accreted onto the core, $\dot{M}$ will decrease, and the protostar will become optically visible. (Alternatively, the envelope might also be dispersed by a strong stellar wind.)

In contrast to the visual and near-infrared region of the spectrum, the envelope will be optically thin at submillimeter wavelengths during most of the collapse phase. Using

$$\frac{Q(\lambda)}{Q(V)} = 10^{-3}\,\frac{100\ \mu m}{\lambda} \tag{10}$$

(Whitcomb et al., 1981) we find

$$\tau(\lambda) = 0.8\left(\frac{T_o}{10\ K}\right)^{3/2}\left(\frac{M_c}{1M_\odot}\right)^{-1/2}\left(\frac{R_{ev}}{10^{13}\ cm}\right)^{-1/2}\left(\frac{\lambda}{100\ \mu m}\right)^{-1} \tag{11}$$

It is precisely this point that makes a space-borne, far-infrared and submillimeter telescope such an ideal instrument for studying the star-formation process. Figures 2 and 3 show the results of a numerical calculation of the spherically symmetric collapse of a 1-$M_\odot$ cloud, immediately after the formation of the hydrostatic core, and during the last stage of the collapse (Winkler, 1978). From a detailed comparison, we see that the approximations discussed above are in good agreement with these numerical results.

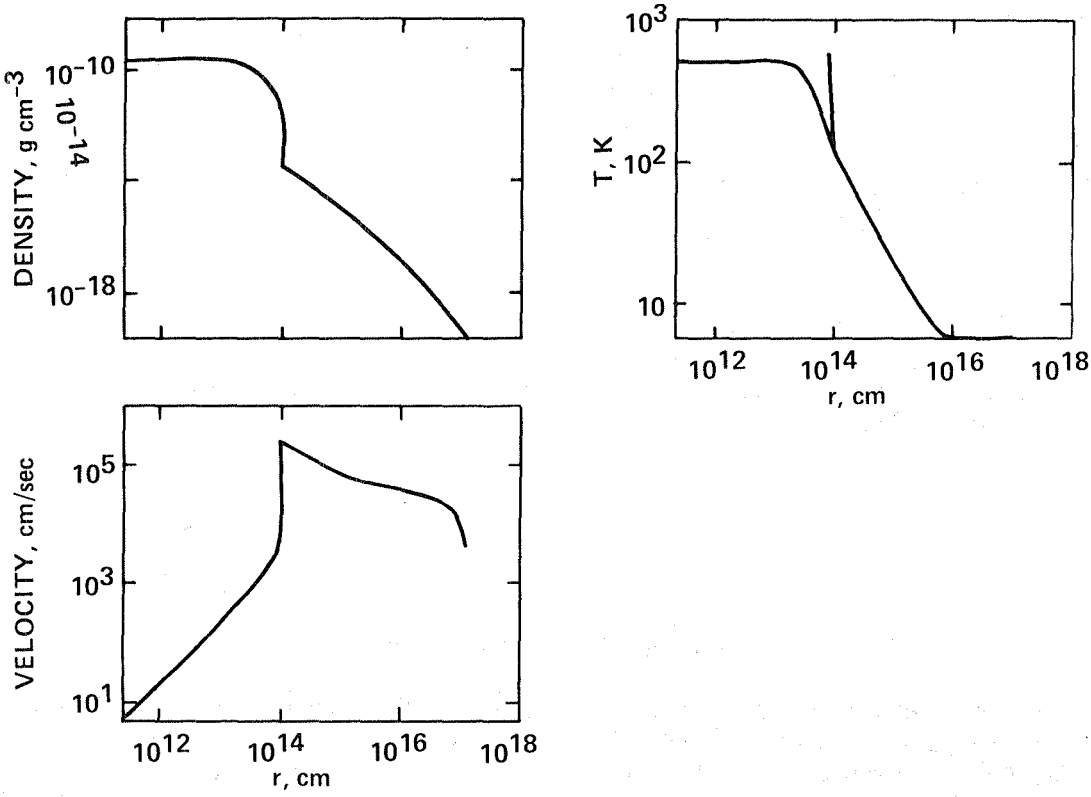

Figure 2.- Velocity, temperature, and density distribution of a 1-$M_\odot$ protostar immediately after the formation of the hydrostatic core (Winkler, 1978).

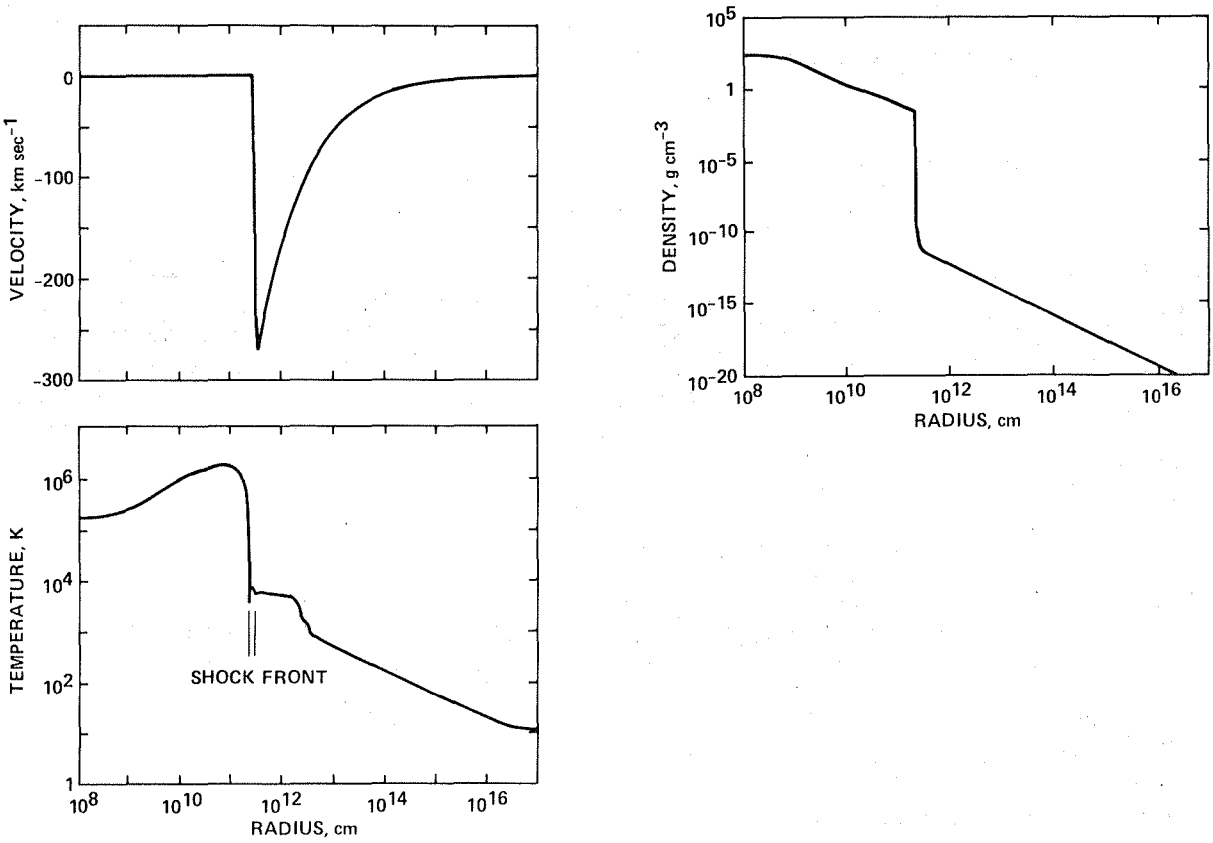

Figure 3.- Velocity, temperature, and density distribution of a 1-$M_\odot$ protostar at the end of the main accretion phase. The hydrostatic core contains 99.3% of the total mass (Winkler, 1978).

Collapse of Rotating Clouds

Up to now we have only considered the spherically symmetric collapse of a cloud. If, however, the parent molecular cloud has angular momentum, then the star-formation process will be somewhat different. A collapsing, rotating cloud will form a core and a circumstellar disk in the center, surrounded by a freely falling envelope. Figure 4 shows a schematic of the different zones in a collapsing rotating cloud; table 3 gives their characteristic properties. Note that there will be an accretion shock on the disk as well as on the core. As a result, there will be a range of shock velocities, depending on the position in the disk.

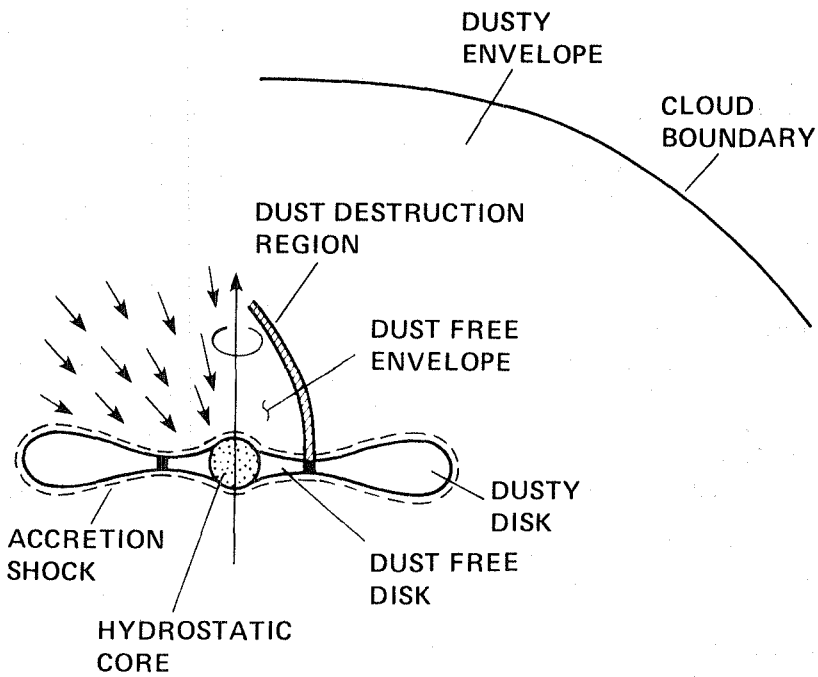

Figure 4.- A schematic of the structure of a collapsing, rotating cloud.

TABLE 3.- SIZES OF DIFFERENT ZONES IN A COLLAPSING ROTATING CLOUD

Zone	R, cm
Central core	3×10^{10}
Dust-free disk	10^{13}
Dusty disk	10^{14}
Dust-free envelope	10^{13}
Dusty envelope	10^{17}

The mass in the disk, relative to that in the core, is very sensitive to the ratio of the accretion rate to the angular momentum transport rate in the disk (Cassen and Summers, 1983). Thus, the thin-disk model of Lin (1981) and the fat-disk model of Cameron (1978) for the proto-planetary disk around the early Sun are characterized by small and large rate ratios, respectively.

This difference bears directly on the basic problem of planet formation. In a thin-disk model, planet formation starts with the condensation of small (submicron-sized) dust grains. These dust grains, and possibly interstellar grains which escaped destruction, coagulate. The resulting large (centimeter-sized) grains will decouple from the gas and settle in the midplane of the disk. The planets are then built up from this thin disk of dust (Safronov, 1972). This gradual process of planet formation is, however, believed to be slow ($\sim10^8$ yr), particularly for the outer planets.

In contrast, in a fat-disk model, planet formation is initiated by gravitational instabilities in the disk. In this way, dense clumps are formed, which contract upon themselves and form the planets (Cameron, 1978). However, this model for planet formation also has some drawbacks. In particular, special mechanisms are needed to produce nonsolar abundances in the terrestrial planets (Wetherill, 1978). Furthermore, it might be difficult to form a rocky core inside the giant planets (Cameron, 1984: personal communication).

Many hydrodynamical studies have been performed on the collapse of rotating clouds. Most of these were, however, concerned with studying the development of ring, bar, and numerical instabilities. Essentially, no self-consistent numerical hydrodynamical calculations have been performed on which the collapse of a rotating interstellar cloud is followed all the way to stellar densities. This contrast with the one-dimensional case merely reflects the increased complexity of the additional dimension. Quite a lot of theoretical effort has also been devoted to the study of circumstellar disks around protostars, once the disks have been formed. This work is generally based on the viscous accretion disk models of Lynden-Bell and Pringle (1974). The surface density and photospheric temperature calculated from such a simple analytical model for the solar nebula are shown in figure 5 (Cassen and Summers, 1983). For this case, the angular momentum is 5×10^{51} g·cm^2/sec, a so-called "minimum-angular-momentum" nebula (e.g., the minimum angular momentum found by taking the observed angular momentum in the solar system and correcting to solar abundances).

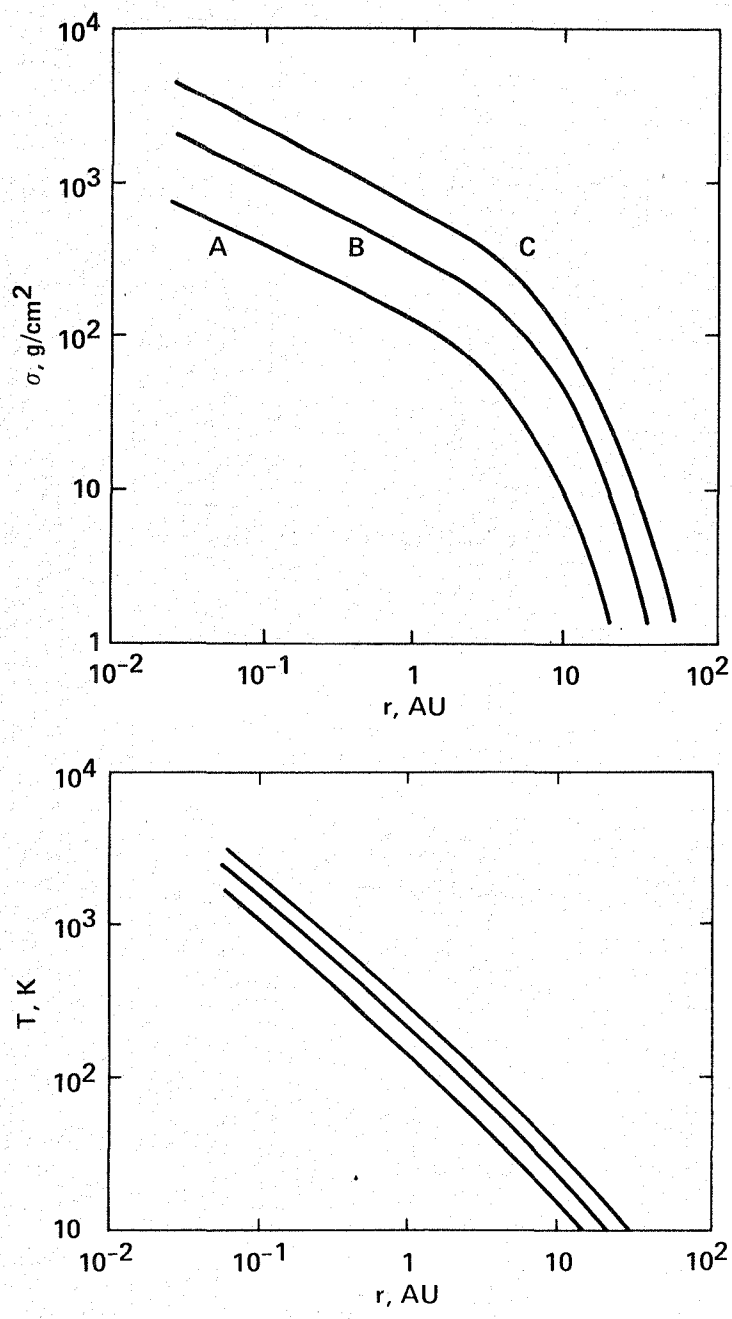

Figure 5.- Surface density and temperature of a "minimum-angular-momentum" solar nebula (Cassen and Summers, 1983). The models A, B, and C correspond to times of 0.5, 1, and 1.6×10^5 years, respectively.

Mass-Loss from Low-Mass Protostars

The presence of strong stellar winds in T Tauri stars was suggested as early as 1962 on the basis of the P Cygni profile in Hα in some T Tauri stars (Herbig, 1962). The best evidence for mass-loss from T Tauri stars comes from molecular observations. Carbon-monoxide observations in the vicinity of T Tauri stars and other pre-main-sequence, low-mass stars reveal blue-shifted and red-shifted emissions in two opposing

lobes (Snell and Edwards, 1981). The observed outflow velocities in these low-mass stars are of the order of 15 km/sec or less. Emission from shocked, vibrationally excited H_2 has also been detected from the vicinity of low-mass protostars (Simon and Joyce, 1983). Evidence for outflow is also seen in the motion of Herbig-Haro (HH) objects associated with low-mass protostars. Proper-motion studies and line studies of HH objects reveal velocities up to 400 km/sec (Herbig and Jones, 1981; Graham and Elias, 1983). The proper-motion vector of the HH objects points back to the exciting star.

The picture that emerges from the wealth of data available, is one of protostars losing mass at a high rate. The resultant stellar wind is channeled, quite close to the star, into two opposing lobes, possibly by a circumstellar disk. This fast (~400-km/sec) wind accelerates the HH objects. The impact on the surrounding molecular cloud material causes two shocks to occur. First, the wind will shock against the shell of swept-up material (i.e., the wind shock, v ~ 400 km/sec); second, this shell of swept-up material will be driven supersonically into the molecular cloud (i.e., the molecular shock, v ~ 15 km/sec).

Large Deployable Reflector

As discussed before, the main advantage of the LDR in studying star formation derives from the fact that the collapsing envelope of a protostar is only optically thin for wavelengths longer than about 100 μm (eq. (11)). Currently, the LDR is envisioned as a 20-m-diam dish, diffraction-limited to 30 μm. This implies a beam size at 100 μm of 1.0 arcsec. At the distance of the nearest site of star formation, the Taurus clouds (150 pc), this corresponds to 2.0×10^{15} cm (100 AU). Inspection of tables 1-3 reveals that the LDR can easily resolve the collapsing envelope. However, the core and the disk around it cannot be resolved. Studies of structures in proto-planetary disks (planet formation) need a resolution of at least a few astronomical units. Such a resolution could be achieved with an interferometer with a baseline of 1 km. The diameter of each element of such an interferometer could be limited to 4 m. A large number of such elements (~25) could then make up for the smaller collection area of the individual elements relative to the 20-m design. However, linking such an interferometer may present some difficulties. Furthermore, such an interferometer will not have the same near-infrared light-bucket possibilities as the 20-m design. It should be emphasized that although a 20-m, far-infrared telescope will not be able to resolve the core and disk, it still will be an extremely important instrument for studies of star formation. In the next two sections, this will be illustrated on the basis of possible far-infrared continuum and line emission studies with such an instrument.

3. CONTINUUM EMISSION STUDIES

Infrared continuum emission is due to warm ($T_d \approx 10\text{-}10^3$ K) dust grains. The dust in collapsing molecular clouds can be heated to these temperatures through either absorption of photons or viscous friction with the gas. The former situation arises in the radiative transport in the circumstellar envelope of the protostar, and the latter may occur in a viscous accretion disk around the protostellar core.

The Envelope

The spectral appearance of a collapsing nonrotating protostellar cloud with a total mass of 3 $M_\odot$ is shown in figure 6. The different models are identified in table 4. These spectra have been computed by solving the coupled equations of gas and dust hydrodynamics and radiative transfer (Bertout and Yorke 1978). During most of the collapse phase of the parental cloud, the spectrum peaks in the far-infrared.

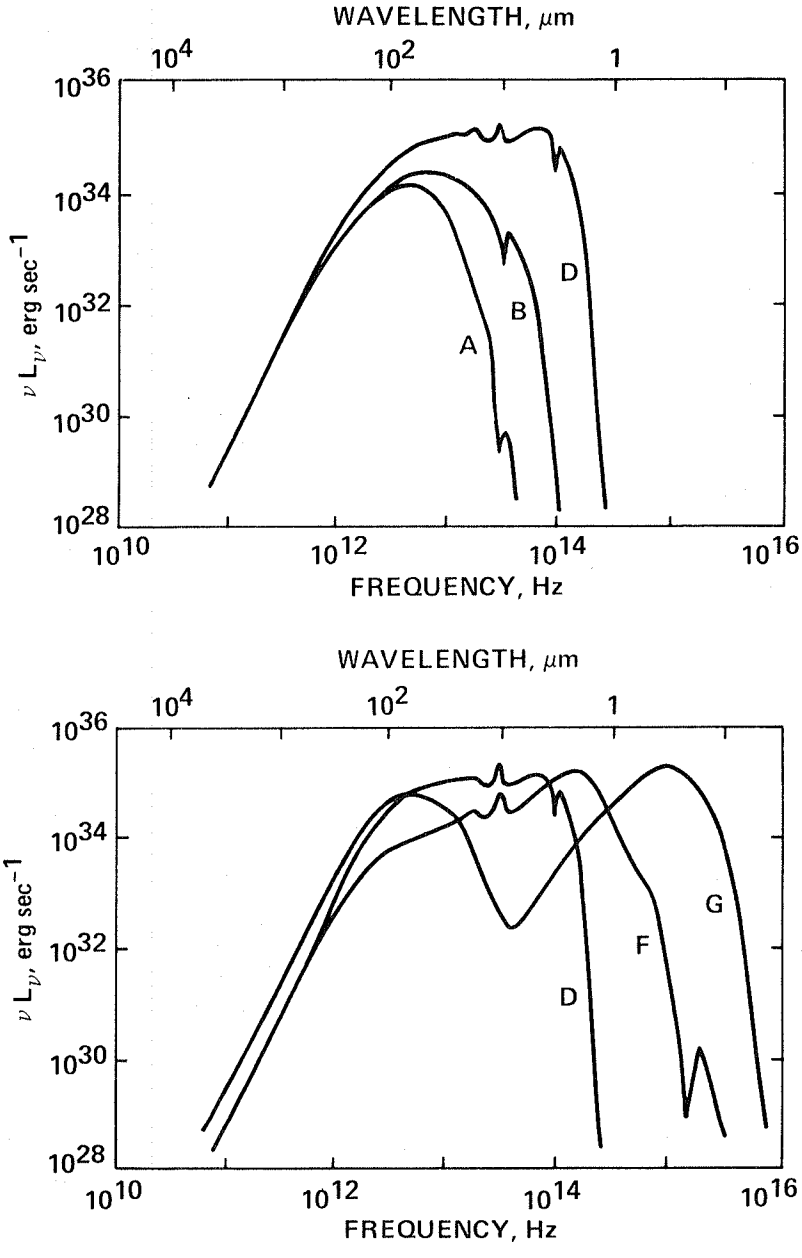

Figure 6.- The spectral appearance of a collapsing, nonrotating, 3-$M_\odot$ cloud at different time steps: models A-G, table 4 (Bertout and Yorke, 1978).

Only in the last phase of the collapse ($\Delta t \geqq 10^6$ yr) does the newly formed star become optically visible. In effect, this reflects the high optical depth of the dust in the envelope for UV, visible, and near-infrared radiation (sec. 1 and table 4). The emission will, therefore, be dominated by the cold dust at the outside, which radiates predominantly in the far-infrared.

The intensity distribution as a function of impact parameter p at four selected wavelengths is given in figure 7 (Yorke, 1980). These are calculated for model F in table 4. At a distance of 150 pc (the distance to the nearest region of low-mass-star formation in Taurus), the diameter at 30 μm (≈2 AU) is about 0.01", which is much less than the diffraction limit of the LDR at that wavelength (0.3"). At 125 μm, the computed angular size is about 1", comparable to the LDR diffraction limit.

The calculated total flux at 100 μm is 2×10^{22} erg·sec^{-1}·Hz^{-1}. Assuming an LDR detection limit of 2×10^{-3} Jy at 100 μm at a resolution of $\nu/\Delta\nu = 10$, the LDR will make these sources observable out to a distance of about 100 kpc. Besides our own galaxy, this includes the Large Magellanic Clouds (LMC) and Small Megellanic Clouds (SMC). At that distance, 1" corresponds to about 0.25 pc, and multiple sources may cause some confusion along the line of sight. If it is assumed that the space density of T Tauri stars in the LMC and SMC is equal to that observed in the entire Taurus-Auriga complex (e.g., about 0.5 pc^{-3}, Jones and Herbig, 1979) and that the T Tauri phase lasts 10 times longer than the collapse phase, a mean separation between collapsing protostars of about 2.5 pc is obtained. This is a much larger separation than the beam size of the LDR and is comparable to the size of dark Lynds clouds (~5 pc) in the Taurus-Auriga region. For the denser concentrations of T Tauri stars in this complex, the space density is about 8 pc^{-3} (Myers, 1982) leading to a mean separation of 1.1 pc. This is still much larger than the diffraction limit of the LDR at 100 μm; some confusion along the line of sight may occur in this case however.

The Disk

The calculation of the spectral appearance of a collapsing protostar discussed above was performed assuming spherical symmetry. In actuality, a circumstellar disk will likely evolve (sec. 1). The presence of a circumstellar disk will modify the

TABLE 4.- CORE AND ENVELOPE PARAMETERS OF A COLLAPSING SPHERICALLY SYMMETRIC 3 M PROTOSTELLAR CLOUD AT VARIOUS EVOLUTIONARY TIMES AFTER THE FORMATION OF A CENTRAL CORE

Model	Time after core formation, 10^3 yr	M_{core}, $M_\odot$	L, $L_\odot$	$\dot{M}$, 10^{-6} $M_\odot$/yr	A_V, magnitude
A	18	0.46	8	15.6	4712
B	67	.97	15	8.2	1183
C	156	1.52	24	5.0	580
D	332	2.12	111	2.3	147
E	598	2.50	90	.94	66
F	1170	2.85	97	.33	17
G	1345	2.90	96	.20	.66

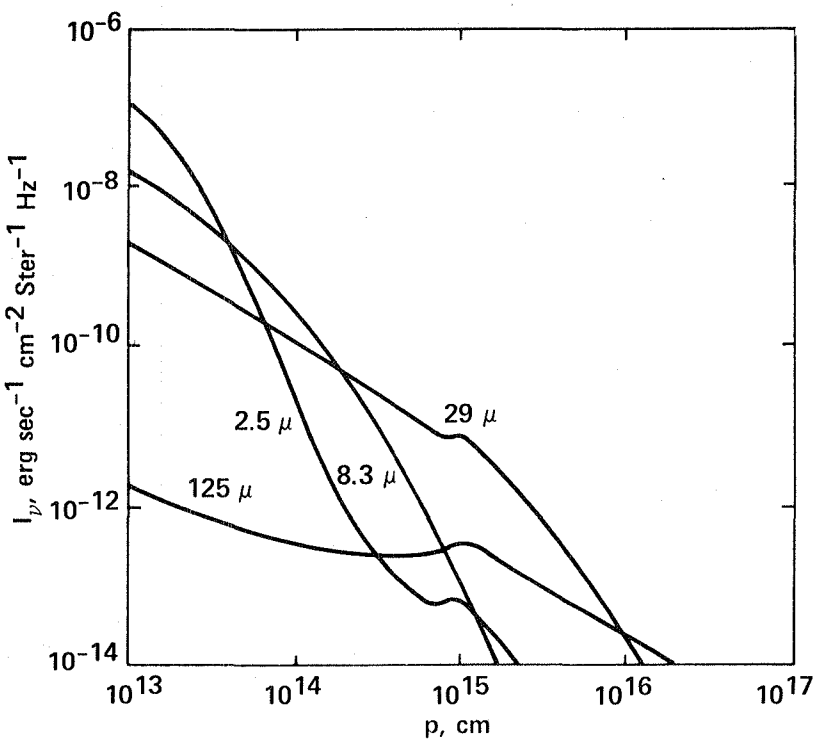

Figure 7.- Surface brightness as a function of impact parameter for a collapsing, nonrotating 3-$M_\odot$ cloud: model F in table 4 (Yorke, 1980).

previously discussed results for the radiative transfer, and the disk may be observable in the far-infrared. We will now calculate the spectrum of a viscous accretion disk, neglecting radiative transfer through the circumstellar envelope. This assumption makes the calculation relatively easy.

First, it should be noted that the disk is optically thick out to a wavelength of about 1 mm. Assuming that the far-infrared properties of the dust in the disk are similar to those of dust in molecular clouds (Whitcomb et al., 1981), we find

$$\tau(\lambda) = 0.4\left(\frac{\lambda}{100\ \mu m}\right)^{-1} \sigma \tag{12}$$

for $\lambda \geq 30$ μm, where σ is the surface density of the disk in grams per square centimeter. Thus, for a "minimum-angular-momentum" disk (fig. 5) we find an optical depth at 1 mm of 4 at a radius in the disk of 10 AU.

Second, an approximation of the photospheric temperature of the disk is given by $T = T_{ev}R_{ev}/r$, where T_{ev} is the evaporation temperature of the dust and R_{ev} is the radius in the disk at which the dust will evaporate. The observed infrared emission at a frequency ν from such a disk at a distance D is now given by

$$S_\nu = \int I_\nu \, d\Omega = 2\pi\left(\frac{R_{ev}\cos\theta}{D}\right)^2 \int_1^{X_{max}} I_\nu(X) X \, dX \tag{13}$$

where X is equal to r/R_{ev}; R_{max} is the outer radius of the disk; and the cosine factor takes into account projection effects (Beall et al., 1984). The specific intensity $I_\nu(X)$ is given by the Planck function at temperature $T(X)$. This yields

$$S_\nu = 4\pi\left(\frac{R_{ev}\cos\theta}{D}\right)^2\left(\frac{kT_{ev}}{h\nu}\right)^2 \frac{h\nu^3}{c^2}\left[D(Y_{max}) - D(Y_{ev})\right] \qquad (14)$$

where $Y(X)$ is given by

$$Y(X) = \frac{h\nu}{kT(X)} \qquad (15)$$

and $D(Y)$ is the function

$$D(Y) = \int_0^Y \frac{t}{e^t = 1}\, dt \qquad (16)$$

tabulated in Abramowitz and Stegun (1970). Figure 8 shows the calculated spectrum of a proto-planetary disk for $R_{ev} = 6\times10^{12}$ cm (e.g., the radius of Mercury), $R_{max} = 10$ AU, $T_{ev} = 10^3$ K (e.g., the evaporation temperature of silicate material), $\theta = 45°$ and $D = 150$ pc (e.g., the distance to Taurus). For comparison, the spectrum of a 4000-K blackbody with a luminosity of 30 $L_\odot$ is also shown. The disk spectrum is much broader than a blackbody owing to the dust temperature gradient. The presence of multiple dust components, each with its own temperature gradient, will further broaden this spectrum. The total luminosity of the viscous accretion disk is about 5 $L_\odot$. This is, however, highly dependent on the assumed inner radius and the condensation temperature. It should be emphasized that the spectrum shown in figure 8 will be further modified by radiative transfer in the circumstellar envelope. As discussed in section 1, the circumstellar envelope will be optically thick for wavelengths less than about 100 μm; thus the disk is only observable at far-infrared and submillimeter wavelengths.

During the subsequent evolution of the protostar, the disk has to disappear again rapidly ($\Delta t \sim 10^6$ yr), because optically visible T Tauri stars do not show the excess infrared (10-μm) emission associated with a viscous disk (Cohen and Witteborn, 1984: in preparation). This disappearance can be due to several processes, including angular momentum transport from the protostar to the disk causing the disk to expand, accretion of the disk into larger ($\geq$1 cm) objects reducing the surface area of solid particles, or disruption of the disk through interaction with a powerful stellar wind. Our present knowledge of the star-formation process is insufficient to distinguish between these possibilities. It should, perhaps, be noted here that the dusty disk around Vega (recently discovered in the far-infrared by IRAS (Aumann et al., 1984), is probably not a direct remnant of the protostellar accretion disk. These particles may be similar to (though possibly larger than) the particles in the zodiacal cloud around the Sun.

Flattened dust distributions have been recently observed in the far-infrared looking toward several T Tauri stars, using the Kuiper Airborne Observatory (KAO). Figure 9 shows a 100-μm map of the source SSV 13 (Cohen et al., 1984: in preparation). The KAO has resolved this source in one direction. The direction of the outflow of the HH objects is perpendicular to the major axis of the flattened dust distribution.

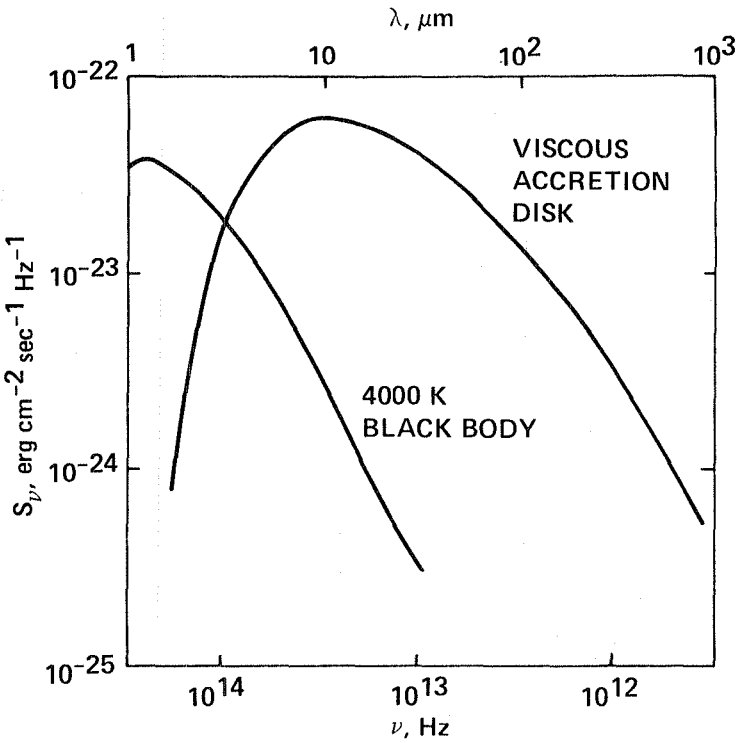

Figure 8.- The spectral appearance of a viscous accretion disk (solar nebula). For comparison a 4000 K blackbody with a total luminosity of 30 $L_{\odot}$ is also shown.

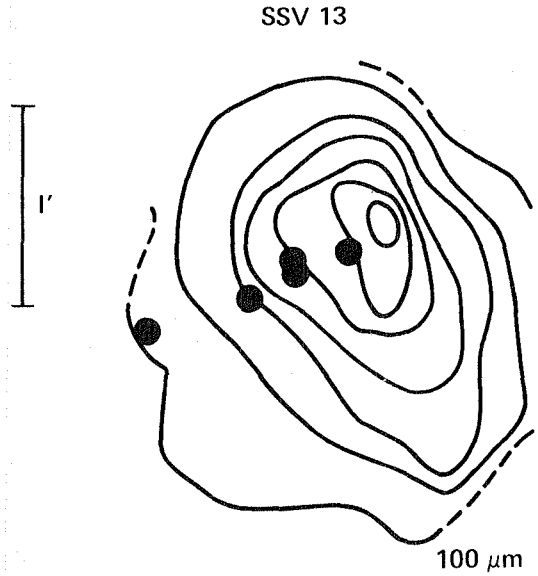

Figure 9.- A 100-μm map of the source SSV 13, obtained with the KAO. The black dots represent Herbig-Haro objects (Cohen et al., 1984).

It is tempting to identify this flattened distribution with the envelope of a collapsing rotating protostar. With the LDR, it will be possible to resolve such structures easily and to study the interaction of a strong stellar wind with the envelope.

Summary

Summarizing the discussion on the continuum infrared emission of low-mass protostars, we conclude that the LDR will be able to detect the IR continuum of a 3-$M_\odot$ collapsing protostar out to a distance of 100 kpc. Although it is projected that the Shuttle Infrared Telescope Facility (SIRTF) will be able to detect protostars throughout the galaxy, its larger beam size at 100 μm will present some viewing confusion problems for distances of the order of 10 kpc or larger. Its smaller beam size at shorter wavelengths will not be of much help, because the spectrum of a collapsing protostar peaks so strongly at about 100 μm. For the later phases of the collapse ($\Delta t \geq 10^5$ yr), SIRTF will be a good instrument for studying the near-infrared emission. Although the LDR will not be able to resolve the protostellar core or its circumstellar disk, it will be able to resolve the collapsing envelope.

4. LINE EMISSION STUDIES

In this section we discuss line emission from the collapsing envelope, the accretion shock on the core and the circumstellar disk, and the shocks driven by the stellar wind. Each of these is associated with a particular velocity, and high spectral resolving power ($\nu/\Delta\nu \sim 10^3$-10^5) is imperative for a meaningful study.

The Collapsing Envelope

The gas in the circumstellar envelope of the collapsing protostar is heated by gas-grain collisions, and by IR photon excitation followed by collisional deexcitation. The gas is cooled by emission in molecular rotational and vibrational transitions. It is important to note that only those regions that are optically thin in the dust continuum at a particular wavelength can be probed by emission or absorption line studies at that wavelength.

The far-infrared molecular line emission from molecular clouds during the isothermal collapse phase has been calculated by several groups (e.g., de Jong et al., 1975; Gerola and Glassgold, 1978). Figure 10 shows the calculated infrared spectrum of a collapsing cloud with a hydrogen density of 10^4 cm^{-3}, a size of 3 pc, and a systematic velocity gradient of 1 $km \cdot sec^{-1} \cdot pc^{-1}$ for gas temperatures of 20 K (fig. 10(a)) and 80 K (fig. 10(b)) (de Jong et al., 1975; Dalgarno et al., 1974). For comparison, the expected continuum from dust with the same temperature is also shown. During this phase of the collapse the cloud is still optically thin in the dust continuum, so even the emission lines below 100 μm could be detectable with high enough spectral resolution. It is interesting to note that molecules like HCl, H_2O, and HD can be important coolants of a collapsing molecular cloud despite their low abundance (Dalgarno et al., 1974; Goldsmith and Langer, 1978).

The intensity of the molecular cooling lines is quite high, which makes them detectable even in nearby galaxies. As an example, consider the $J = 8 \rightarrow 7$ transition in CO at 325 μm. The computed integrated line intensity in a 3" beam for the

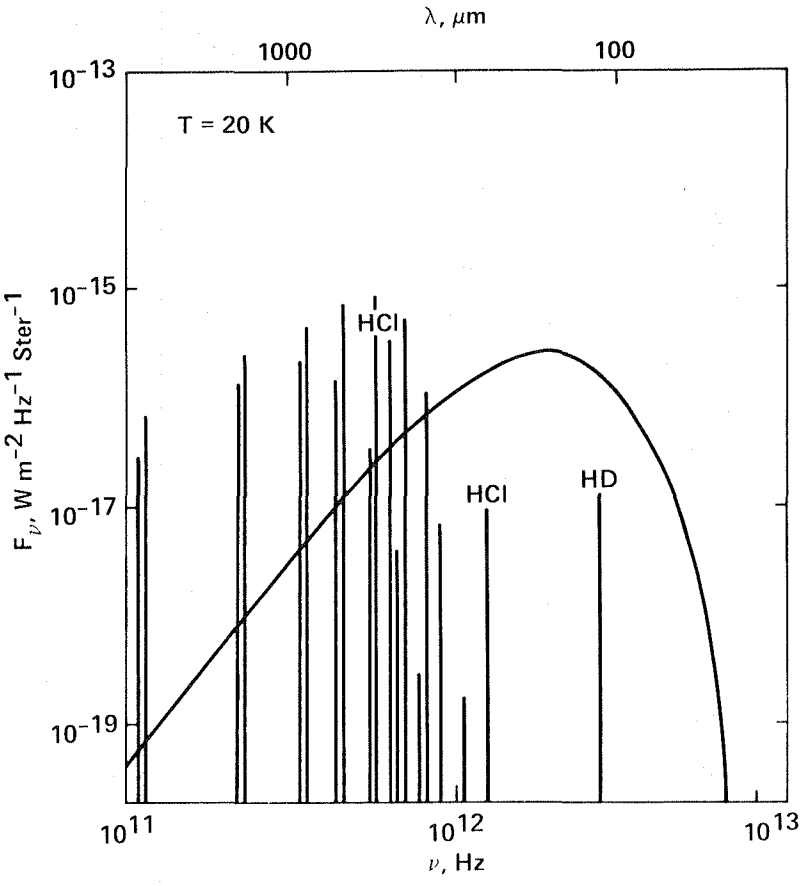

Figure 10.- Intensities of molecular rotation lines in a collapsing interstellar cloud at 20 K and 80 K. The line pairs are the different rotational transitions of ^{13}CO (left) and ^{12}CO (right). The other lines are identified in the figure. The solid line represents dust emission at the same temperature (de Jong et al., 1975).

80-K case is about 2.5×10^{-17} W/m^2. That makes this particular line detectable with the LDR out to a distance of about 1 Mpc, which includes all galaxies in the local group. Here we have assumed a spectral resolving power of 10^5, a signal-to-noise ratio of 5, and a 25-sec integration time.

Essentially, no calculations have been performed for the expected cooling line-emission of the collapsing protostellar envelope beyond the isothermal phase. Of course, the envelope will be optically thick in the visible and near-infrared during this phase. Because of the higher gas temperatures in the envelope during this phase, an even richer far-infrared line spectrum is expected. The scale size of the emitting region is now, however, much smaller ($\leq10^{16}$ cm). This is still larger than the diffraction limit of the LDR at 100 μm out to a distance of 1 kpc. It will, therefore, be possible to study in detail the density, temperature, and chemical structure, and the velocity field in the circumstellar envelope of protostars in the Taurus-Auriga clouds during this collapse phase. Such a study will contribute considerably to our understanding of the physical and chemical processes in collapsing molecular clouds.

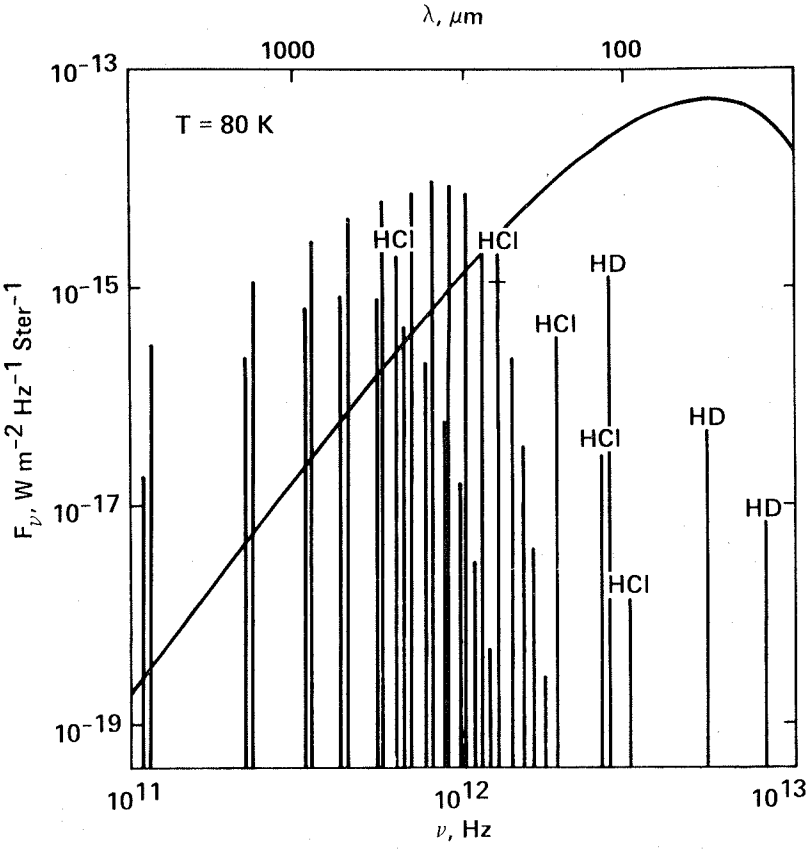

Figure 10.- Concluded.

The Accretion Shocks

Besides these thermal emission lines from the circumstellar envelope, emission lines from the accretion shock will also be present. In the initial phase, the shock velocity is still less than 25 km/sec, and molecules will not be dissociated. Most of the kinetic energy of in-fall will be radiated away in the far-infrared rotational lines of H_2, CO, HD, OH, and H_2O. Consider, for example, the collapse of a 1-$M_\odot$ cloud immediately after the formation of the hydrostatic core (fig. 2). The velocity of the accretion shock at that time is only 2.5 km/sec. We estimate the total luminosity of this shock to be about 2×10^{-3} $L_\odot$ (of eq. (4)). If we assume that this energy is radiated by about 100 lines (probably an overestimate), then the flux per line from such a cloud in Taurus is about 3×10^{-17} W/m^2. With a line width of 2.5 km/sec, they are much brighter than the continuum. This makes them easily observable with the LDR.

As time increases, the velocity of the accretion shock increases. For shock velocities above 50 km/sec, molecules will be dissociated, and the atomic fine-structure lines of O I, O III, Si II, and Fe II will be the only lines of the shocked gas that might be detectable in the far-infrared. However, these lines dominate the cooling only below about 5000 K. It is likely that in this phase the temperature of the core is higher than this, in which case these lines would be unobservable. Most of the energy will be radiated away in optical and UV lines, which are absorbed by the circumstellar envelope.

Some of the material in the in-falling envelope will rain in on the disk rather than on the core. The velocity of the accretion shock on the disk will be much less than that on the core. Also, the photospheric temperature of the disk is lower than that of the core. Assuming a mass accretion rate on the disk of 10^{-5} $M_\odot$/yr in an angular ring with a radius and width of 1 AU, and a shock velocity of 10 km/sec yields a shock luminosity integrated over all lines of about 3×10^{32} erg/sec. Most of this energy is expected to be radiated in the low-lying rotational levels of H_2O and CO. Again, assuming that most of the energy is emitted in 100 lines, that the distance is 150 pc, and that the line width is 10 km/sec, we find a line intensity of 10^{-20} erg·cm^{-2}·Hz^{-1}·sec^{-1}. This is much brighter than the continuum of the disk photosphere. Of course, only the far-infrared H_2O lines will be observable because of the high dust opacity in the circumstellar envelope. Again, high resolution is needed to separate these lines from the cooling lines of the infalling envelope.

The Stellar Wind

Finally, we consider line emission from shocks driven by a stong stellar wind. The mass-loss of the protostar will drive two shocks. First, the wind will be shocked (v_w ~ 100 km/sec) when it meets the shell of swept-up material; second, because of the wind pressure, this shell will expand into the molecular cloud, driving a shock of ~10 km/sec. The first shock radiates predominantly in optical and UV lines, although some infrared lines will also be present. Table 5 gives the intensity of far-infrared lines for a 100-km/sec shock incident on a gas with a density of 100 cm^{-3}, and a magnetic field of 1 μG (Shull and McKee, 1979). All of the lines in table 4 are detectable with the LDR, as long as the shock fills the beam. Of these

TABLE 5.- INTENSITIES OF SELECTED INFRARED LINES FOR A SHOCK VELOCITY OF 100 km/sec, A DENSITY OF 100 cm^{-3}, AND A MAGNETIC FIELD STRENGTH OF 1 μG

Species	λ, μm	I, erg·cm^{-2}·sec^{-1}·sr^{-1}
C II	158	2.1×10^{-6}
O I	63	1.1×10^{-4}
O I	145	1.3×10^{-5}
O III	88	1.4×10^{-6}
O III	52	7.4×10^{-6}
Si II	35	4.9×10^{-5}
S III	34	5.5×10^{-6}

Notes: These intensities are taken from Shull and McKee (1979). The numerical integrations are terminated at a temperature of 500-800 K. Consequently, an additional 0.06-0.1 eV per H atom will be radiated in the fine structure lines of Si II, O I, and C II.

lines, the O I (63-μm) line is the most interesting. It has been shown that the intensity of this line is directly proportional to the mass-loss rate of the protostar,

$$I(63\ \mu m) = 10^{-13}\ n_w v_w\ \text{erg cm}^{-2}\ \text{sec}^{-1}\ \text{sr}^{-1} \qquad (17)$$

where n_w and v_w are the preshock density and velocity of the wind in cgs units (Hollenbach, 1984). This makes studies of this line particularly interesting.

The low velocity of the shell shock ensures that most of the energy is radiated in infrared lines. Table 6 gives the intensity of some of these lines for a 10-km/sec shock incident on a molecular cloud with a density of 10^4 cm^{-3} and a magnetic field of 50 μG (Draine et al., 1983). Again, these lines are bright enough to be observable with the LDR, as long as the shock fills the beam. It should be noted that the relative intensities of these lines are sensitive to the postshock temperature and density and, therefore, to the shock velocity, the preshock density, and the magnetic field strength.

TABLE 6.- INTENSITIES OF SELECTED INFRARED LINES FOR A SHOCK VELOCITY OF 10 km/sec, A DENSITY OF 10^4 cm^{-3} AND A MAGNETIC FIELD STRENGTH OF 50 μG

Species	λ, μm	I, erg·cm^{-2}·sec^{-1}·sr^{-1}
OI	63	2.5×10^{-4}
OI	145	1.2×10^{-5}
CI	609	1.7×10^{-6}
CI	370	1.7×10^{-5}
H_2 v=0 S(0)	28	9.0×10^{-6}
S(1)	17	1.3×10^{-4}
S(2)	12	3.2×10^{-5}
S(3)	9.7	2.0×10^{-5}

These intensities are taken from Draine et al. (1983).

One interesting project would be to map HH objects in these lines. The LDR has high enough spatial resolution to easily resolve a typical HH object (~10"). High-frequency resolution is needed to separate the wind shock from the shell shock, and to study the velocity field. In this way, the interaction between the wind and the molecular gas can be probed in detail. Among other things, this may help clarify the energy and momentum transfer from a stellar wind to a molecular cloud. In particular, it may elucidate the nature of HH objects.

Summary

We conclude that the LDR will be a powerful tool for studying line emission from protostellar objects because of its high angular and frequency resolution. Important studies can be made of the temperature, density and chemical structure, as well as the velocity field in collapsing envelopes, the accretion shock on their cores and circumstellar disks, and of the shocks driven by the stellar wind.

REFERENCES

Abramowitz, M.; and Stegun, I. A.: Handbook of Mathematical Functions. Dover Publications, New York, 1970.

Aumann, H. H.; Gillett, F. C.; et al.: Discovery of a Shell around Alpha Lyrae. Astrophys. J. (in press), 1984.

Beall, J. H.; Knight, F. K.; et al.: Infrared Emission From Accretion Disks: Detectability and Variability. Astrophys. J. (in press), 1984.

Bertout, C.; and Yorke, H. W.: The Spectral Appearance of Solar-Type Collapsing Protostellar Clouds. Protostars and Planets, T. Gehrels, Ed., University of Arizona Press, Tucson, Ariz., 1978, pp. 648-689.

Cameron, A. G. W.: Physics of the Primitive Solar Nebula and of Giant Gaseous Protoplanets. Protostars and Planets, T. Gehrels, ed., University of Arizona Press, Tucson, Ariz., 1978, pp. 453-487.

Cassen, P.; and Summers, A.: Models of the Formation of the Solar Nebula. Icarus, vol. 53, 1983, pp. 26-40.

Dalgarno, A.; de Jong, T.; Oppenheimer, M.; and Black, J. H.: Hydrogen Chloride in Dense Interstellar Clouds. Astrophys. J., vol. 192, 1974, pp. L37-40.

de Jong, T.; Chu, S. I.; and Dalgarno, A.: Carbon Monoxide in Collapsing Interstellar Clouds. Astrophys. J., vol. 199, 1975, pp. 69-78.

Draine, B. T.; Roberge, W. G.; and Dalgarno, A.: Magnetohydrodynamic Shock Waves in Molecular Clouds. Astrophys. J., vol. 264, 1983, pp. 485-507.

Evans, N. J.: Star Formation in Molecular Clouds. Protostars and Planets, T. Gehrels, ed., University of Arizona Press, Tucson, Ariz., 1978, pp. 153-164.

Gerola, H.; and Glassgold, A. E.: Molecular Evolution of Contracting Clouds: Basic Methods and Initial Results. Astrophys. J. Suppl. Ser., vol. 37, 1978, pp. 1-45.

Goldsmith, P. F.; and Langer, W. D.: Molecular Cooling and Thermal Balance of Dense Interstellar Clouds. Astrophys. J., vol. 222, 1978, pp. 881-895.

Graham, J. A.; and Elias, J. H.: Herbig-Haro Objects in the Dust Globule ESO 210-6A. Astrophys. J., vol. 272, 1983, pp. 615-626.

Herbig, G. H.: The Properties and Problems of T. Tauri Stars and Related Objects. Adv. Astron. Astrophys., vol. 1, 1962, pp. 47-103.

Herbig, G. H.; and Jones, B. F.: Large Proper Motions of the Herbig-Haro Objects HH1 and HH2. Astron. J., vol. 86, 1981, pp. 1232-1244.

Hollenbach, D.: Mass Loss Rates From Protostars and OI (63-μm) Shock Luminosities. Icarus (in press), 1984.

Jones, B. F.; and Herbig, G. H.: T Tauri Stars in the Taurus-Auriga Complex. Astron. J., vol. 84, 1979, pp. 1872-1889.

Larson, R. B.: Collapse Calculations and Their Implications for the Formation of the Solar System. On the Origin of the Solar System, H. Reeves, ed., CNRS, Paris, France, 1972, pp. 142-150.

Larson, R. B.: The Stellar State: Formation of Solar-Type Stars. Protostars and Planets, T. Gehrels, ed., University of Arizona Press, Tucson, Ariz., 1978, pp. 43-57.

Lin, D. N. C.: Convective Accretion Disk Model for the Primordial Solar Nebula. Astrophys. J., vol. 246, 1981, pp. 972-984.

Lynden-Bell, D.; and Pringle, J. E.: The Evolution of Viscous Disks and the Origin of the Nebular Variables. Mon. Nat. R. Astron. Society, vol. 168, 1974, pp. 603-637.

Martin, R. N.; and Barrett, A. H.: Microwave Spectral Lines in Galactic Dust Globules. Astrophys. J. Suppl. Ser., vol. 36, 1978, pp. 1-34.

Mestel, L.: Theoretical Processes in Star Formation. Star Formation, T. de Jong and A Maeder, eds., Reidel, Dordrecht, Holland, 1977, pp. 213-247.

Myers, P. C.: Low-Mass Star Formation in the Dense Interiors of Barnard 18. Astrophys. J., vol. 257, 1982, pp. 620-632.

Myers, P. C.: Dense Cores in Dark Clouds. III. Subsonic Turbulence. Astrophys. J., vol. 270, 1983, pp. 105-118.

Myers, P. C.; and Benson, P. J.: Dense Cores in Dark Clouds. II. NH_3 Observations and Star Formation. Astrophys. J., vol. 266, 1983, pp. 309-320.

Safronov, V. S.: Evolution of the Protoplanetary Cloud and the Formation of the Earth and Planets. IPST, Jurusalem, Israel, 1972.

Salpeter, E. E.: Formations and Destruction of Dust Grains. Annu. Rev. Astron. Astrophys., vol. 15, 1977, pp. 267-293.

Shu, F. H/: Self-Similar Collapse of Isothermal Spheres and Star Formation. Astrophys. J., vol. 214, 1977, pp. 488-502.

Shull, J. M.; and McKee, C. F.: Theoretical Models of Interstellar Shocks. I. Radiative Transfer and UV Precursors. Astrophys. J., vol. 227, 1979, pp. 131-149.

Simon, T.; and Joyce, R. R.: Observations of H_2 Emission from Molecular Clouds and Herbig-Haro Objects. Astrophys. J., vol. 265, 1983, pp. 864-876.

Snell, R. L.: A Study of Nine Interstellar Dark Clouds. Astrophys. J. Suppl. Ser., vol. 45, 1981, pp. 121-151.

Snell, R. L.; and Edwards, S.: High Velocity Molecular Gas near Herbig-Haro Objects in HH 7-11. Astrophys. J., vol. 251, 1981, pp. 103-107.

Solomon, P. M.: Physics of Molecular Clouds From Millimeter Wave Line Observations. Infrared Astronomy, G. Seti and G. G. Fazio, eds., Reidel, Dordrecht, Holland, 1978, pp. 97-114.

Spitzer, L.: Physical Processes in the Interstellar Medium. Wiley, New York, 1978.

Stahler, S. W.; Shu, F. H.; and Taam, R. E.: The Evolution of Protostars. I. Global Formulation and Results. Astrophys. J., vol. 241, 1980, pp. 637-654.

Wetherill, G. W.: Accumulation of the Terrestrial Planets. Protostars and Planets, T. Gehrels, ed., University of Arizona Press, Tucson, Ariz., 1978, pp. 565-598.

Whitcomb, S. E.; Gatley, I.; et al.: Far-Infrared Properties of Dust in the Reflection Nebula, NGC 7023. Astrophys. J., vol. 246, 1981, pp. 416-425.

Winkler, K. H. A.: Late Stages of Solar Type Protostars. The Moon and Planets, vol. 19, 1978, pp. 237-266.

Yorke, H. W.: The Evolution of Protostellar Envelopes of Masses 3 $M_\odot$ and 10 $M_\odot$. II. Radiation Transfer and Spectral Appearance. Astron. Astrophys., vol. 85, 1980, pp. 215-220.

1. Report No.	2. Government Accession No.	3. Recipient's Catalog No.
NASA TM 85960		

4. Title and Subtitle	5. Report Date
STUDIES OF LOW-MASS STAR FORMATION WITH THE LARGE DEPLOYABLE REFLECTOR	June 1984
	6. Performing Organization Code: ATP
7. Author(s): A. G. G. M. Tielens and D. J. Hollenbach	8. Performing Organization Report No.: A-9754
	10. Work Unit No.: T-3252
9. Performing Organization Name and Address: Ames Research Center, Moffett Field, California 94035	11. Contract or Grant No.
	13. Type of Report and Period Covered: Technical Memorandum
12. Sponsoring Agency Name and Address: National Aeronautics and Space Administration, Washington, DC 20546	14. Sponsoring Agency Code: 159-41-01

15. Supplementary Notes

Point of contact: David Hollenbach, M/S 245-6, Ames Research Center, Moffett Field, Calif. 94035, (415) 965-6426 or FTS 448-6426

16. Abstract

Estimates are made of the far-infrared and submillimeter continuum and line emission from regions of low-mass star formation. The intensity of this emission is compared with the sensitivity of the Large Deployable Reflector (LDR), a large space telescope designed for this wavelength range. LDR will be able to probe the temperature, density, and chemical structure, and the velocity field of the collapsing envelopes of these protostars. LDR will be able to study the accretion shocks on the cores and circumstellar disks of low-mass protostars, and will be able to detect shock waves driven by protostellar winds.

17. Key Words (Suggested by Author(s))	18. Distribution Statement
Star formation Protostars Infrared Large Deployable Reflector	Unlimited Subject Category - 90

19. Security Classif. (of this report)	20. Security Classif. (of this page)	21. No. of Pages	22. Price*
Unclassified	Unclassified	27	A03

*For sale by the National Technical Information Service, Springfield, Virginia 22161

End of Document